PNAS BRIEF REPORT | BIOPHYSICS AND COMPUTATIONAL BIOLOGY OPEN ACCESS

Optical sectioning of unlabeled samples using bright-field microscopy

Braulio Gutiérrez-Medina[a,1]

Edited by David Weitz, Harvard University, Cambridge, MA; received December 21, 2021; accepted March 7, 2022

The bright-field (BF) optical microscope is a traditional bioimaging tool that has been recently tested for depth discrimination during evaluation of specimen morphology; however, existing approaches require dedicated instrumentation or extensive computer modeling. We report a direct method for three-dimensional (3D) imaging in BF microscopy, applicable to label-free samples, where we use Köhler illumination in the coherent regime and conventional digital image processing filters to achieve optical sectioning. By visualizing fungal, animal tissue, and plant samples and comparing with light-sheet fluorescence microscopy imaging, we demonstrate the accuracy and applicability of the method, showing how the standard microscope is an effective 3D imaging device.

three-dimensional microscopy | optical sectioning | bright field | label-free imaging | image processing

The classic bright-field (BF) microscope is an indispensable tool in any biological laboratory, routinely used to evaluate cellular or tissular morphology in stained two-dimensional (2D) samples. In the absence of staining, however, BF images of phase objects display little contrast (1). Several imaging modalities address this limitation, from early alternatives now widespread (e.g., Zernike phase contrast and differential interference contrast) (2) to recent advancements that allow quantitative measurement of the complex sample field (e.g., quantitative phase contrast) (3).

Despite drawbacks, BF remains attractive because it is a simple, fast, and inexpensive microscopy method, where photodamage and phototoxicity is much reduced compared to fluorescence microscopy. Three-dimensional (3D) imaging in BF has been obtained by processing multiple images acquired from different angles into a single reconstruction (4, 5) or using deep learning to predict 3D fluorescence signal (6, 7), although specialized instrumentation or extensive computer modeling is required.

Broadly, the reconstruction of an input object from the corresponding output image constitutes a well-known inverse problem in microscopy. Deconvolution, a standard method that addresses this problem, typically analyzes images in the Fourier domain and has been successfully applied to BF in 2D (8, 9). Here, we introduce optical sectioning in bright-field microscopy (OSBM), a 3D image reconstruction method based on analyzing in real space high-contrast BF images of phase objects.

Results

In BF with Köhler illumination (Fig. 1*A*), decreasing the numerical aperture (NA) of the condenser, establishing the coherent regime ($NA_{condenser}/NA_{objective} = \varsigma \rightarrow 0$) (2, 10), results in high-contrast imaging of phase specimens and strong contrast inversion upon axial scanning through focus. This behavior is evident in the phase point spread function (pPSF) (8, 9) (Fig. 1*B*); Weber contrast of the central spot changes from positive to negative and is zero at exact focus ($z = 0$). However, by introducing an amount of defocus close to the depth of field we find that BF imaging is in good correspondence with a ground truth (Fig. 1*C* and *SI Appendix*), suggesting accurate sample information can be extracted from BF.

An inverse-imaging problem is therefore identified, where BF image stacks featuring axial intensity gradients constitute the output signal. We reconstruct the input 3D object by finding the axial location of the source of these gradients, using standard digital processing filters (11). The set of points thus found corresponds to the scattering structures that compose the specimen.

The OSBM procedure comprises operating a BF microscope under Köhler illumination ($\varsigma = 0.1$ to 0.2), capturing a z-stack of images of unstained samples, and applying the following digital pipeline to images (Fig. 1*D*). First, large spatial structures are filtered out from raw BF images. Second, the z-gradient is computed by performing pairwise image subtraction, followed by Gaussian smoothing. Finally, a filter that

Author affiliations: [a]Division of Advanced Materials, Instituto Potosino de Investigación Científica y Tecnológica, 78216 San Luis Potosí, Mexico

Author contributions: B.G.-M. designed research, performed research, contributed new reagents/analytic tools, analyzed data, wrote the paper, and received funds to perform research.

Competing interest statement: B.G.-M. is inventor on USPTO patent application 17/550,797 submitted by Instituto Potosino de Investigación Científica y Tecnológica A.C. that covers "System and method for three-dimensional imaging of unstained samples using bright field microscopy."

[1]Email: bgutierrez@ipicyt.edu.mx.

This article contains supporting information online at http://www.pnas.org/lookup/suppl/doi:10.1073/pnas.2122937119/-/DCSupplemental.

Published March 28, 2022.

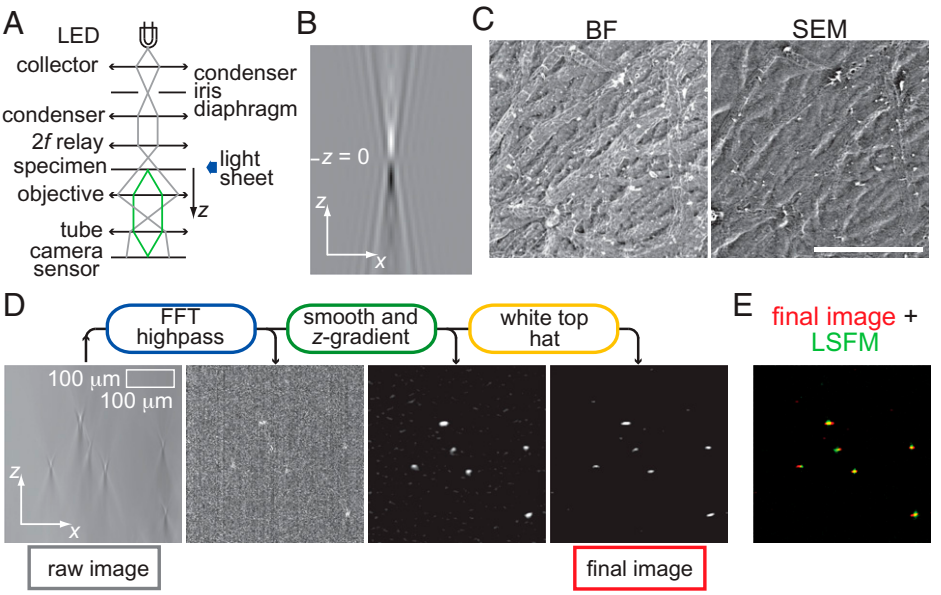

Fig. 1. Principle of OSBM. (*A*) Schematic of our BF microscopy setup, showing illumination and scattered light rays (gray and green, respectively). Lenses are depicted as double arrows. (*B*) Image of the BF pPSF, computed using equation 1 in reference 9 with: $\lambda = 450$ nm, $n = 1.0$, $NA_{objective} = 0.1$; field of view (x–z): 90 × 404 μm^2. (*C*) BF and scanning electron microscopy (SEM) images of a dry filamentous fungus sample (*T. atroviride*). BF image was acquired at $z = -6.0$ μm. (Scale bar: 100 μm.) (*D*) Digital pipeline of OSBM (round boxes) and resulting images for a living *T. atroviride* sample. (*E*) Overlay of the "final image" of OSBM shown in *D* (red) with the corresponding LSFM image (green).

highlights small, bright features (such as white top hat) is applied. Fig. 1*D* shows how OSBM works, applied to a living sample of the filamentous fungus *Trichoderma atroviride*. To validate OSBM, we compare resulting images with true optical sectioning (12) counterparts, using light-sheet fluorescence microscopy (LSFM). The background-free, axially localized spots produced by OSBM show good overlap with those from LSFM (Fig. 1*E*).

To demonstrate 3D imaging using OSBM, we first consider a living filamentous network (*T. atroviride*), where scattering structures are well-localized and mostly distant from each other (compared to filament diameter). Application of OSBM results in a dramatic transition from blurred (original BF) to crisp (final) images (Fig. 2*A*). Excellent agreement is found between OSBM and LSFM (Fig. 2 *A* and *B*), enabling proper 3D rendering of hyphal structures (Fig. 2*C* and Movie S1). As OSBM does not use a narrowly focused laser beam, sharp images throughout the entire field of view are produced, thus complementing LSFM.

Next, we tested a sample with a continuous scattering structure, an optically cleared blood vessel (Fig. 2*D*). The OSBM image of this tissue is pointillistic, where the collective of points provides sharp localization of tissue boundary and structures such as pleats. A comparison between OSBM and LSFM images shows excellent correspondence in overall sample morphology (Fig. 2 *D* and *E*). A 3D reconstruction is shown in Fig. 2*F* and Movie S2.

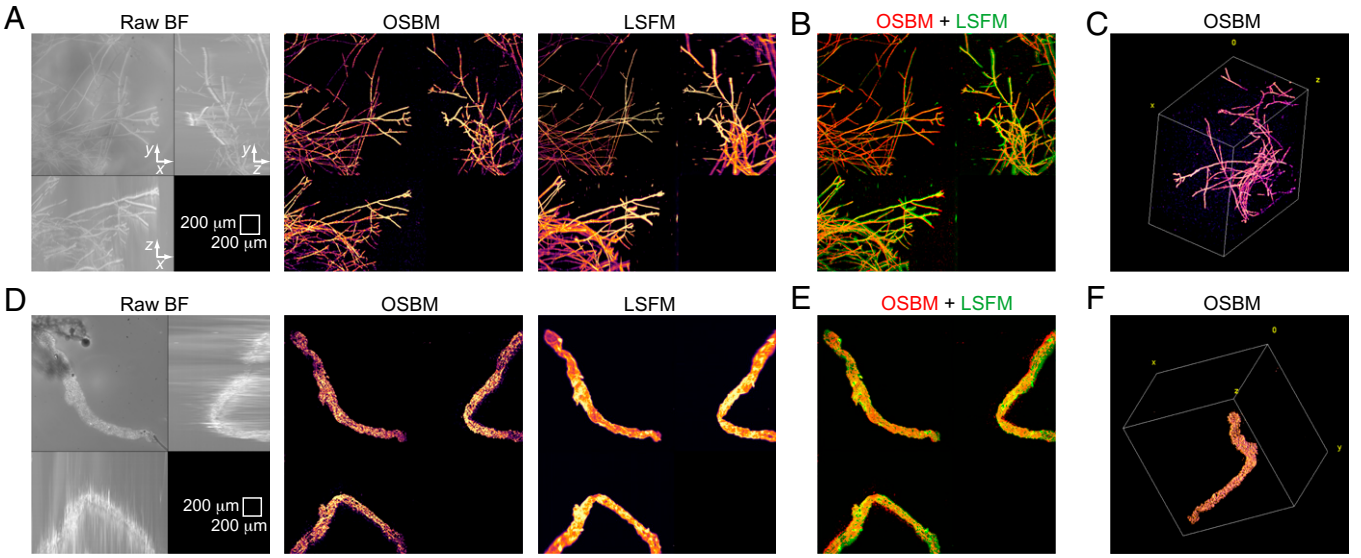

Fig. 2. OSBM imaging for test samples and comparison with LSFM. (*A*–*C*) Fungal sample. (*D*–*F*) Clarified blood vessel sample. (*A* and *D*) Maximum intensity projection (MIP) images for BF, OSBM, and LSFM. (*B* and *E*) Merged images of OSBM (red) and LSFM (green) shown in *A* and *D*, respectively. (*C* and *F*) Three-dimensional images obtained from the corresponding OBSM optical sections. Field of view for *C* and *F*, 1,495 × 1,495 × 1,016 μm^3 and 1,495 × 1,495 × 1,128 μm^3, respectively.

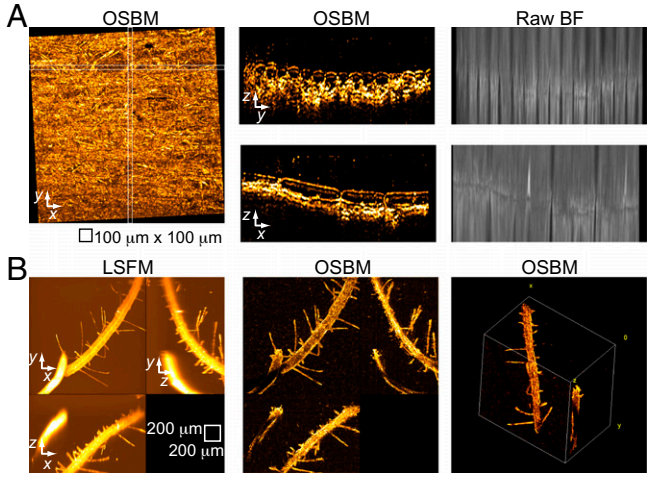

Fig. 3. OSBM imaging of onion skin and plant root. (*A*) OSBM applied to a layer of onion epidermis, showing MIP images along *x*–*y* (*Left*), *y*–*z*, and *x*–*z* (*Center*). *y*–*z* and *x*–*z* images correspond to the white boxes shown in the *x*–*y* projection. BF maximum intensity projection images are shown (*Right*) for comparison. (*B*) Imaging of an unlabeled, untreated *A. thaliana* root sample. Field of view for 3D rendering, 1,495 × 1,495 × 1,008 μm^3.

We applied OSBM to visualize untreated samples with different optical transmissivity. A layer of onion epidermal cells immersed in water is mostly transparent, enabling optimal visualization in BF. Accordingly, we observe the characteristic onion cell shapes in both longitudinal (*x*–*z*) and transversal (*y*–*z*) views (Fig. 3*A*), where periclinal wall curvature is readily identified. A comparison OSBM–LSFM for onion cells (Movie S3) shows good match and consistent cell wall imaging by OSBM in places where fluorescence is absent, emphasizing complementarity between OBSM and LSFM. As onion cell wall thickness is ∼6 μm (13), OSBM can detect isolated semiplanar scattering structures only a few micrometers thick (using a 10× objective lens). Finally, we consider seedlings of *Arabidopsis thaliana*, which present significant optical opacity. By comparing with LSFM, OSBM shows appropriate 3D imaging of thin root hairs and the surface of the thick root that faces the objective lens (Fig. 3*B* and Movie S4). For optically thick biological samples, using infrared light should help improve OSBM imaging (*SI Appendix*).

One limitation for OSBM arises from contrast inversion of the pPSF. When two scattering structures are axially contiguous, they produce overlapped transition regions in the BF image, hindering proper object localization. This effect is expected to be marked for strongly scattering objects such as filaments (scattering intensity $I \propto r^3$, where r is radius of the filament) compared to point-like structures ($I \propto r^6$). In our experiments, we estimate that axial distances below 70 μm (40 μm) between scattering structures cause improper imaging for hyphal (meningeal tissue) samples.

Altogether, OSBM excels at imaging sample boundaries of optically thin objects and structures with low axial spatial density. As a digital extension of traditional BF microscopy and complement to fluorescence microscopy techniques, OSBM offers a simple, direct, and model-free alternative for bioimaging in 3D.

Materials and Methods

Detailed descriptions are provided in *SI Appendix*.

Meningeal tissue was treated using CLARITY (14); optical microscopy and digital image processing were performed using a home-made setup (15) and Fiji (16), respectively.

Data Availability. Image stacks and computer code used to analyze images have been deposited in Zenodo (https://zenodo.org/record/5931508#.YizNqzVMFPY). All other data are included in the manuscript and/or supporting information.

ACKNOWLEDGMENTS. This work was supported by Consejo Nacional de Ciencia y Tecnología (Mexico) Grants IFC-2015-2/1144 and INFR-2018-295138 to B.G.-M. I thank Sergio Casas-Flores, Mitzuko Dautt, Miguel Condés-Lara, and Guadalupe Martínez-Lorenzana for gifts of samples; Ana Iris Peña-Maldonado for help with scanning electron microscopy; the Nanoscience and Nanotechnology Research National Laboratory (LINAN) at Instituto Potosino de Investigación Científica y Tecnológica for access to their facilities; and Isaac Carrillo-Acuña for assistance with fungal sample preparations.

1. F. Zernike, How I discovered phase contrast. *Science* **121**, 345–349 (1955).
2. J. Mertz, *Introduction to Optical Microscopy* (Cambridge University Press, New York, ed. 2, 2011).
3. G. Popescu, *Quantitative Phase Imaging of Cells and Tissues* (McGraw-Hill, New York, 2011).
4. J. Sharpe *et al.*, Optical projection tomography as a tool for 3D microscopy and gene expression studies. *Science* **296**, 541–545 (2002).
5. G. Calisesi *et al.*, Three-dimensional bright-field microscopy with isotropic resolution based on multi-view acquisition and image fusion reconstruction. *Sci. Rep.* **10**, 12771 (2020).
6. C. Ounkomol, S. Seshamani, M. M. Maleckar, F. Collman, G. R. Johnson, Label-free prediction of three-dimensional fluorescence images from transmitted-light microscopy. *Nat. Methods* **15**, 917–920 (2018).
7. E. M. Christiansen *et al.*, In silico labeling: Predicting fluorescent labels in unlabeled images. *Cell* **173**, 792–803.e19 (2018).
8. C. N. Hernández Candia, B. Gutiérrez-Medina, Direct imaging of phase objects enables conventional deconvolution in bright field light microscopy. *PLoS One* **9**, e89106 (2014).
9. B. Gutiérrez-Medina, M. J. Sánchez Miranda, Quantitative image restoration in bright field optical microscopy. *Biophys. J.* **113**, 1916–1919 (2017).
10. G. Stagaman, J. M. Forsyth, Bright-field microscopy of semitransparent objects. *J. Opt. Soc. Am. A* **5**, 648–659 (1988).
11. R. C. Gonzalez, R. E. Woods, *Digital Image Processing* (Pearson, Essex, UK, ed. 4, 2018).
12. J. A. Conchello, J. W. Lichtman, Optical sectioning microscopy. *Nat. Methods* **2**, 920–931 (2005).
13. L. Beauzamy, J. Derr, A. Boudaoud, Quantifying hydrostatic pressure in plant cells by using indentation with an atomic force microscope. *Biophys. J.* **108**, 2448–2456 (2015).
14. G. Martínez-Lorenzana *et al.*, CLARITY with neuronal tracing and immunofluorescence to study the somatosensory system in rats. *J. Neurosci. Methods* **350**, 109048 (2021).
15. B. Gutiérrez-Medina, A. Vázquez-Villa, Visualizing three-dimensional fungal growth using light sheet fluorescence microscopy. *Fungal Genet. Biol.* **150**, 103549 (2021).
16. J. Schindelin *et al.*, Fiji: An open-source platform for biological-image analysis. *Nat. Methods* **9**, 676–682 (2012).